JOURNAL OF GEOPHYSICAL RESEARCH, VOL. 106, NO. D14, PAGES 14,757–14,770, JULY 27, 2001

Identification and separation of Mount Pinatubo and El Niño-Southern Oscillation land surface temperature anomalies

Fanglin Yang[1] and Michael E. Schlesinger

Climate Research Group, Department of Atmospheric Sciences, University of Illinois at Urbana-Champaign, Urbana Illinois

Abstract. Empirical data analyses are performed to detect and separate the signals of the volcanic eruption and El Niño events in the observed surface air temperature (SAT) anomalies over land for the 2 years following the Pinatubo eruption. Composite analyses of surface temperatures for the 1950-1997 period, excluding the 2 years following each of the three major volcanic eruptions, Agung, El Chichón, and Pinatubo, show that the distribution of SAT anomalies over most land areas for the El Niño composite is opposite to that for the La Niña composite. The pattern of SAT anomalies changes from season to season. This feature is more prominent over North America than over the other continents. Singular value decomposition analyses show that following the Pinatubo eruption, El Niño signals were weak over Eurasia but relatively strong over the other continents. Over North America, the 1991-1992 El Niño event contributed more than 50% to the observed surface cooling of about –1.0°C in June, July, and August 1992. Globally averaged, the maximum cooling over land with the El Niño-Southern Oscillation signals removed is –0.5°C in September, October, and November 1992 and September, October, and November 1993.

1. Introduction

The Mount Pinatubo volcano on the island of Luzon (15°N, 120°E), Philippines, erupted catastrophically in June 1991. About 20 x 10^{12} g (20 Tg) of gaseous SO_2 was injected into the stratosphere, which is about 3 times as much as that injected by the El Chichón eruption [*Bluth et al.*, 1992]. The maximum mass loading of stratospheric sulfate aerosol, which was converted from SO_2, estimated by the Stratospheric Aerosol and Gas Experiment (SAGE) II satellite was about 30 Tg in the last few months of 1991 [*McCormick et al.*, 1995]. The background sulfate aerosol mass loading in the stratosphere is usually less than 1 Tg. The aerosol particles converted from the Pinatubo SO_2 injection were suspended in the atmosphere for several years and caused the largest aerosol perturbation to the stratosphere in the twentieth century. The scattering and absorption of solar radiation and the absorption of terrestrial radiation by the Pinatubo aerosol largely disturbed the radiation balance of the atmosphere [*Stenchikov et al.*, 1998; *Andronova et al.*, 1999]. The maximum global mean net radiative forcing at the tropopause calculated by *Andronova et al.* [1999] using a three-dimensional (3-D) radiative-transfer model, allowing the stratospheric temperatures to adjust radiatively, was about –5.5 W/m^2 in December-January-February (DJF) of 1991-1992. The Pinatubo volcanic aerosol radiatively warmed the tropical lower stratosphere and radiatively cooled the troposphere and the Earth's surface [*Stenchikov et al.*, 1998; *Yang*, 2000].

Large changes in surface air temperature (SAT) were observed for a few years following the Pinatubo eruption. *Parker et al.* [1996] showed that in June-July-August (JJA) 1992 the global mean SAT was about 0.5°C lower than the pre-eruption value. Smaller cooling occurred in JJA 1993. In DJF 1991-1992 and DJF 1992-1993, relative warmth occurred over the Northern Hemisphere continents. However, all of these observed SAT changes cannot be explained by the Pinatubo eruption alone. Events such as the El Niños in 1991-1992 and 1993 [*Trenberth*, 1997] complicated the interpretation of these observed changes.

The relative contributions to the observed surface and atmospheric temperature changes of El Niño events and major volcanic eruptions prior to Pinatubo have long been studied. For example, *Angell* [1988] found that with the occurrences of a relatively weak El Niño after the Agung eruption in 1963 and a very strong El Niño after the El Chichón eruption in 1982, the tropospheric temperatures cooled following the Agung eruption but warmed following the El Chichón eruption. *Mass and Portman* [1989] examined the influences on surface temperature of nine major volcanic eruptions during 1883-1982 and the El Niño-Southern Oscillation (ENSO) events that occurred near the times of these eruptions and found that the ENSO signal can either enhance or mask the volcanic signal. After removing the signals of ENSO, they found only modest cooling (~ 0.1° to 0.2°C) for 1 to 2 years following these major eruptions.

For the Pinatubo eruption, a few observational data analyses and numerical model simulations have been carried out to assess and understand its climatic impact [e.g., *Groisman*, 1992; *Hansen et al.*, 1992; *Graf et al.*, 1993; *Kirchner and Graf*, 1995; *Robock and Mao*, 1995; *Parker et*

[1]Now at Environmental Modeling Center, National Centers for Environmental Prediction, Camp Springs, Maryland.

Paper number 2001JD900146.
0148-0227/01/2001JD900146$09.00

al., 1996; *Kirchner et al.,* 1999]; however, only a limited effort has been made to identify and separate the signals of the volcanic eruption and the El Niño events in the observed SAT anomalies. *Robock and Mao* [1995] examined the effect of major volcanic eruptions on surface temperature for the past 140 years, which includes SAT over land and sea surface temperature (SST) over the ocean. They removed the signals of El Niños from the observed surface temperature anomalies by formulating a linear regression between the Southern Oscillation Index (SOI) and the high-pass-filtered surface temperature anomalies. They found that the cooling in the tropics in mid-1992 and mid-1993 was about 0.2°C to 0.3°C, which is smaller than the cooling before the El Niño signals were removed.

In previous studies [*Angell,* 1988; *Mass and Portman,* 1989; *Robock and Mao,* 1995], SOI and area-averaged SST over the eastern tropical Pacific were used to represent and measure the strength of ENSO events, and attention was paid to the area-averaged surface or atmospheric temperature changes following volcanic eruptions. Here we focus on the geographical distributions of the observed SAT and their seasonal characteristics over land during the 3 years following the Pinatubo eruption, together with the corresponding changes in SST over the eastern tropical Pacific. Composite analyses and singular value decomposition (SVD) [*Bretherton et al.,* 1992] are applied to the observed SAT over land and the SST over the ocean for the 1950-1997 period. This is done to identify and separate the signals of El Niño events, La Niña events, and volcanic eruptions from the observed SAT anomalies over land. Special attention is paid to the SAT anomalies over Eurasia and North America in the JJA and DJF seasons for the 2 years following the Pinatubo eruption. A separate paper (F. Yang and M. E. Schlesinger, On the Surface and Atmospheric Temperature Changes following the 1991 Pinatubo Volcanic Eruption - A GCM Study, submitted to *J. Geophys. Res.*, 2001) is devoted to the thermal and dynamical responses of the Earth's atmosphere to the forcings by the Pinatubo eruption and the SST anomalies simulated by the University of Illinois at Urbana-Champaign (UIUC) 24-layer stratosphere/troposphere general circulation model (GCM) [*Yang et al.*, 2000].

The plan of this paper is as follows. The sources of the data are described in section 2. Section 3 presents the SAT and Niño 3.4 indices, followed in section 4 by the composite analyses of SST and SAT over land. The method and results of the SVD analysis are presented in section 5. A summary and discussion are presented in section 6.

2. Data

Over land the SAT analysis by the NASA Goddard Institute for Space Studies (GISS) [*Hansen et al.,* 1999] is used. The NASA/GISS analysis makes use of data collected from about 7000 meteorological stations and covers the time period from 1880 to 1998. Data are presented as temperature anomalies relative to the climatology of 1951-1980 and are on 8000 equal-area grids. These data were projected onto the 4° x 5° latitude-longitude grid of the UIUC 24-layer atmospheric GCM [*Yang et al.*, 2000] before use. For the purpose of performing statistical analyses, missing data over land between 50°S and 90°N were filled by using adjacent data. Over Antarctica there were a lot of missing data between 1950 and 1997. No attempts were made to correct them.

Two different sets of monthly mean SST anomalies were used to create a uniform set of SST anomalies for 1950-1997. The first set is the reconstructed Reynolds SST provided by the National Oceanic and Atmospheric Administration-Cooperative Institute for Research in Environmental Sciences (NOAA-CIRES) Climate Diagnostics Center (CDC). It covers the time from 1950 to 1992 and the latitudes from 45°S to 69°N with a 2° x 2° resolution. It was reconstructed by fitting in situ data for 1950-1992 based on dominant empirical-orthogonal functions, which were produced by the optimum interpolation analyses of in situ SSTs from 1950-1981 [*Reynolds and Smith,* 1995; *Smith et al.,* 1996]. The second set is the monthly mean Reynolds SST, also provided by the NOAA-CIRES CDC. It includes in situ and satellite SSTs and sea ice coverage data [*Reynolds and Smith,* 1994]. It covers the time from November 1981 to 1998 and has a 1° x 1° resolution over the ocean. We combined the data from 1993 through 1997 of the second set with the data from 1950 through 1992 of the first set to create a new data set for 1950-1997. The resulting SST data were projected onto the 4° x 5° grid of the UIUC 24-layer atmospheric GCM. Monthly mean SST anomalies were derived for 1950-1997 in relation to the SST climatology of *Reynolds and Smith* [1995]. The derived SST anomalies are accurate only between 42°S and 66°N.

3. Indices of Surface Temperature Anomalies

The GISS SAT data set covers the land, including lakes between 50°S and 90°N. Globally averaged SAT over land was higher during the 1980s-1990s than during the 1950s-1970s. This long-term variation is caused by the increasing greenhouse gas concentration in the atmosphere, some other external forcings, and natural variability of the climate [*Andronova* and *Schlesinger,* 2000]. Embedded in this long-term trend are variations with timescales shorter than 10 years that have large amplitudes.

To reveal the short-term variations of SAT over land and their possible relations with El Niños and volcanic eruptions, we applied a high-frequency-pass Lanczos digital filter [*Duchon,* 1979] to the time series of the monthly mean SAT anomalies over land at each grid point to remove variations with timescales longer than 10 years. Figure 1 shows the Niño 3.4 index we calculated by using the unfiltered monthly mean SST anomalies area averaged over the region (5°S–5°N, 120°–170°W) and the index of the high-pass-filtered global mean monthly mean SAT anomalies area averaged over all land except Antarctica for 1950-1997. Before plotting, a 3-month running mean filter was applied to each of the indices. The occurrences of the three major tropical volcanic eruptions, Agung, El Chichón, and Mount Pinatubo, are also marked in Figure 1.

Following *Trenberth* [1997], El Niño and La Niña events are defined here such that the Niño 3.4 index (Figure 1a) is larger than +0.4°C and smaller than –0.4°C, respectively, and lasts at least 6 months. There are 16 such El Niño events and 9 La Niña events between 1950 and 1997. Though the SAT index (Figure 1b) shows rather large interannual and intraseasonal variations, in general there is a distinguishable correspondence between the Niño 3.4 index and the SAT index; that is, usually during El Niño events, positive SAT anomalies are observed, and during La Niña events, negative SAT anomalies are observed.

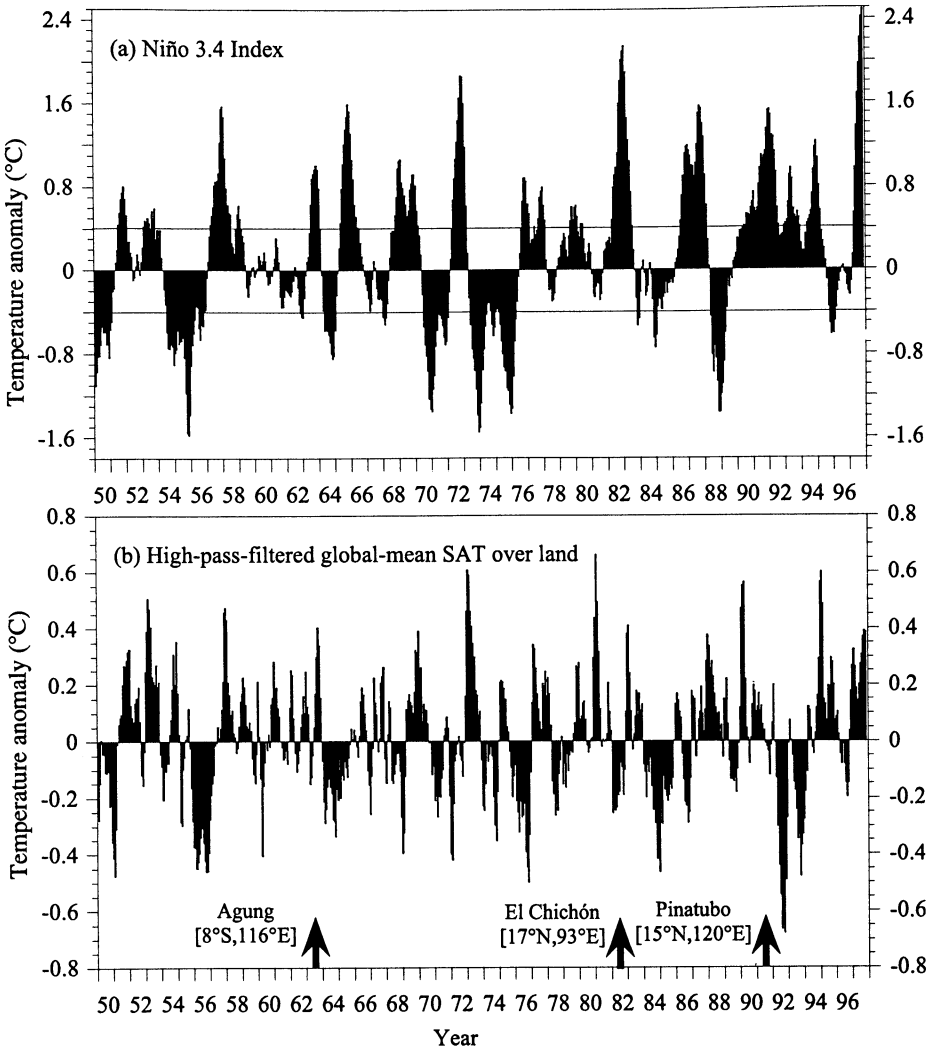

Figure 1. (a) Niño 3.4 index. An event with the index larger than +0.4°C (smaller than −0.4°C) for at least 6 consecutive months is defined as an El Niño (La Niña) event. (b) High-pass-filtered monthly mean SAT anomalies area averaged over all land except Antarctica. Volcanic eruptions of Agung, El Chichón, and Mount Pinatubo are marked in Figure 1b.

Of course, not all the observed SAT anomalies can be explained by El Niño and La Niña events. Other factors, such as the SST anomalies in the North Pacific and North Atlantic and volcanic eruptions, also influence the SAT. The 1982-1983 El Niño was the second largest El Niño event during 1950-1997, but the observed SAT anomalies were below normal in 1982 and only moderately above normal in 1983. This mismatch between the SAT index and the Niño 3.4 index was probably caused by the El Chichón volcanic eruption in 1982. Following the 1991 Pinatubo eruption, large surface cooling appeared in JJA 1992 and JJA 1993, even though there were two El Niños between 1991 and 1993.

4. Composite Surface Temperature Anomalies

We showed in section 3 that there is a connection between the global mean SAT over land and the Niño 3.4 index. Before we quantitatively determine the SAT anomalies induced by El Niño events and exclude them from the observed SAT anomalies over land after the Pinatubo eruption, we examine here the geographical distributions of the observed SAT anomalies over land and SST anomalies over the ocean in El Niño and La Niña years and after volcanic eruptions.

First, for each season March-April-May (MAM), JJA, September-October-November (SON), and DJF we count separately the number of El Niño and La Niña occurrences during 1950-1997. A season with at least 2 months falling in the period of an El Niño (La Niña) event is counted as an El Niño (La Niña) season. Table 1 lists the numbers of El Niño and La Niña occurrences during 1950-1997 for each season and the number of El Niño and La Niña occurrences within the 2 years following each of the three major volcanic eruptions being excluded, the March 1963 Agung eruption, the April 1982 El Chichón eruption, and the June 1991 Mount Pinatubo eruption. Since El Niño events occurred after all three major volcanic eruptions, the number of El Niño occurrences drops considerably after the volcano years are excluded, but the number of La Niña occurrences remains almost unchanged.

Table 1. Number of El Niño and La Niña Seasons During 1950-1997

Season	El Niño	El Niño Excluding Volcanic Years	La Niña	La Niña Excluding Volcanic Years
MAM	13	9	9	9
JJA	14	9	10	9
SON	17	14	12	11
DJF	15	12	12	11

Second, for each season we compute the composite surface temperature anomalies, SAT over land and SST over the ocean, for each of the 16 categories listed in Table 1. Figure 2 presents the global distributions of surface temperature anomalies in JJA and DJF for the El Niño and La Niña composites, each with the volcano years excluded, and for the volcano composite which contains 6 years of data and includes the 2 years following each of the three major volcanic eruptions.

Over the ocean, in both JJA and DJF, the distribution of SST anomalies for the El Niño composite (Figures 2a and 2d) is opposite to that for the La Niña composite (Figures 2b and 2e), not only in the middle to eastern tropical Pacific as expected, but also in some other regions of the ocean. For the El Niño composite, the SST anomalies are negative in the western tropical Pacific and the middle to high-latitude Pacific in both hemispheres and are positive for the La Niña composite. Over the Indian Ocean, positive SST anomalies are observed for the El Niño composite and negative SST anomalies for the La Niña composite. For each composite, the SST anomaly patterns in all seasons are similar (figures for MAM and SON are not shown).

Over land, in both JJA and DJF, the distribution of SAT anomalies for the El Niño composite is almost everywhere opposite to that for the La Niña composite. Unlike the pattern of SST anomalies, the pattern of SAT anomalies changes with season. In JJA, for the El Niño composite, negative SAT anomalies occur over Europe, northern Asia, South Africa, and northern North America except Alaska, and positive SAT anomalies occur over South America, southern Asia, the Middle East, and Africa. For the La Niña composite, almost exactly opposite distributions of SAT anomalies to the El Niño composite are found over these regions. In DJF, for the El Niño composite, positive SAT anomalies exist almost everywhere over land, except over northern Eurasia, southeastern North America, and eastern Greenland. Opposite distributions of SAT anomalies are found again over these regions for the La Niña composite. The SAT anomaly is generally larger in DJF than in JJA. The largest SAT anomalies occur in the Northern Hemisphere high latitudes. The opposite distributions of SAT anomalies between the El Niño and La Niña composites are also found in MAM and SON (not shown).

We calculated the pattern correlation coefficients between the El Niño and La Niña composites for SAT anomalies over land and SST anomalies over the ocean for each of the four seasons, with and without the six volcanic years included. The results are shown in Table 2, case 1. We used the Monte Carlo method to test the statistical significance of the pattern correlation coefficients. For example, to test if the correlation –0.731 shown in Table 2 for SAT in DJF was statistically significant, we randomly drew 23 years out of the total 48 years of DJF data with volcanic years excluded, constructed two composites (one using the first 12 years of randomly drawn data and the other using the remaining 11 years of randomly drawn data), and calculated the pattern correlations between these two composites for SAT and SST. The numbers 12 and 11 correspond to the years of El Niño and La Niña seasons in DJF found in the total 48 years, with the six volcanic years excluded (Table 1). The procedure was repeated for 10,000 times (the Monte Carlo test). We found that 1.1% of the correlation coefficients obtained from the Monte Carlo test were smaller than –0.731. Consequently, the correlation –0.731 is statistically significant at the 1.1% level. We used one-sided criteria for all the Monte Carlo tests except for SAT in cases 2 and 3 in Table 2 where two-sided criteria were used since the signs of the correlations cannot be determined. The calculated correlation coefficients are larger in magnitude for SST than for SAT. For SAT, higher correlation coefficients are obtained after excluding the six volcano years. The correlations for SAT and SST between the El Niño and La Niña composites are all statistically significant at about or better than the 5% level, except for SAT in MAM with the volcanic years included.

In both JJA and DJF the volcano composite (Figures 2c and 2f) is different from either the El Niño composite or the La Niña composite. Over the ocean the distribution of SST anomalies for the volcano composite is similar to that for the El Niño composite. This is because El Niño events occurred at the time of the three major volcanic eruptions. However, over land the distribution of SAT anomalies for the volcano composite is different from that for the El Niño composite. The difference is larger in DJF than in JJA. In JJA, large negative SAT anomalies are found over all the continents, except North Africa and northern South America. In DJF, large positive SAT anomalies are found over central Eurasia and central North America, and large negative SAT anomalies are found over North Africa and southwestern and northeastern North America. We also calculated and present in Table 2 the pattern correlation coefficients between the volcano composite and the El Niño composite and between the volcano composite and the La Niña composite for SAT anomalies over land and SST anomalies over the ocean for each of the four seasons. Volcanic years are excluded from the El Niño and La Niña composites. The correlation coefficients are all much smaller in magnitude than those between the El Niño and La Niña composites.

The observed surface temperature anomalies after volcanic eruptions presented here, with the low-frequency variability being filtered, consist not only of the influence of volcanic aerosols but also other external forcing and internal climate variations of the ocean-atmosphere system, such as El Niño events and the North Atlantic Oscillation. The opposite distributions of surface temperature anomalies between the El

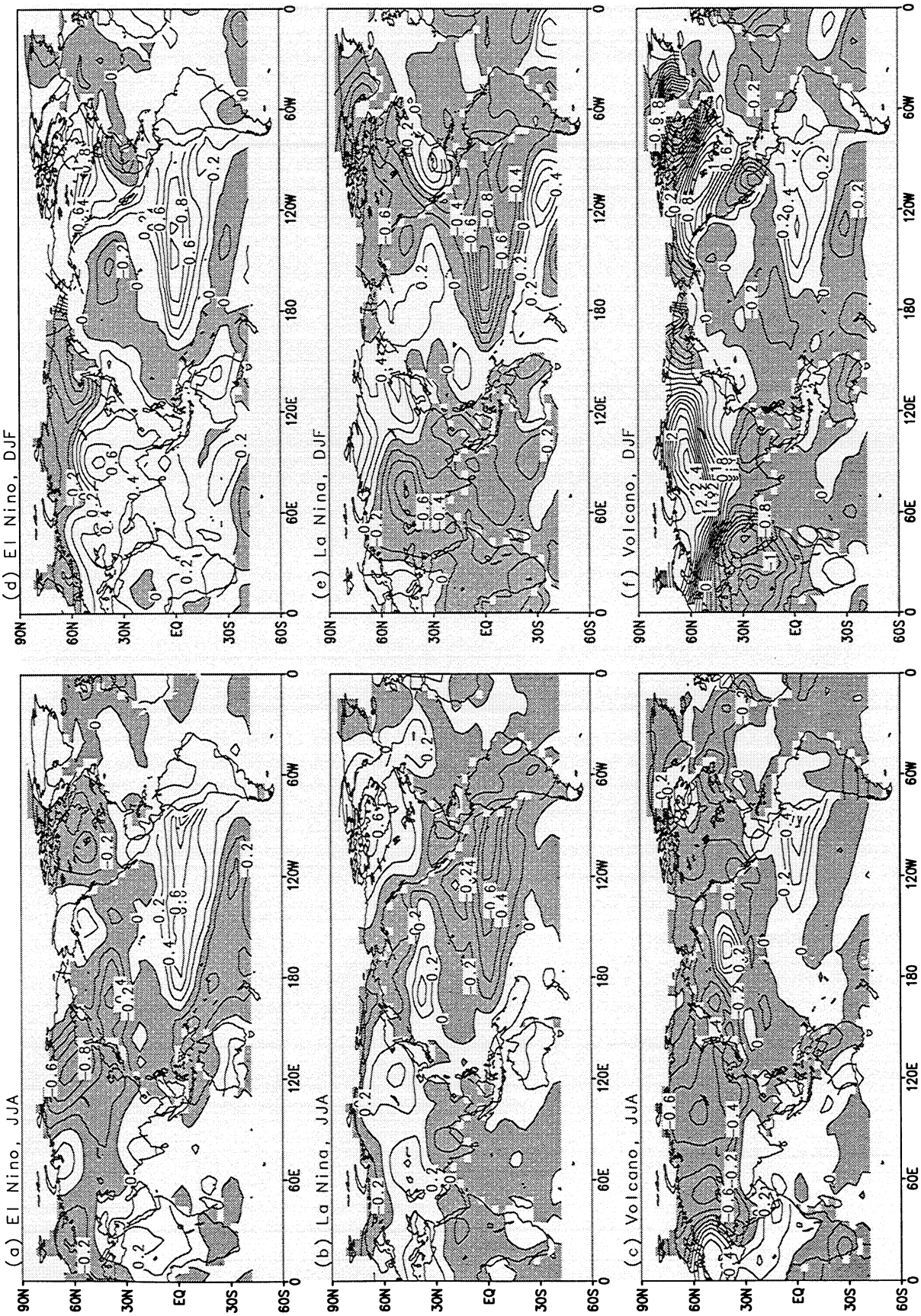

Figure 2. Surface temperature anomalies in (a,b,c) JJA and (d, e, f) DJF for (a, d) the El Niño composite and (b, e) the La Niña composite with volcano years excluded and for (c, f) the volcano composite. The contour interval is 0.2°C. Negative anomalies are shaded.

Table 2. Pattern Correlation Coefficients Between (Case 1) El Niño and La Niña Composites With (WV) and Without (WOV) the 6 Volcano Years Included, (Case 2) the Volcano and El Niño Composites, and (Case 3) the Volcano and La Niña Composites, for SST Anomalies Over the Ocean and SAT Anomalies Over Land[a]

Season	El Niño / La Niña (Case 1)				Volcano / El Niño (Case 2)		Volcano / La Niña (Case 3)	
	SAT		SST		SAT	SST	SAT	SST
	WV	WOV	WV	WOV				
MAM	–0.420	–0.556	–0.660	–0.685	0.158	0.536	–0.046	–0.361
	(14.3%)	(4.0%)	(0.1%)	(0.1%)	(60.4%)	(0.2%)	(87.2%)	(4.6%)
JJA	–0.422	–0.526	–0.720	–0.722	0.378	0.423	–0.136	–0.330
	(0.5%)	(0.3%)	(0.1%)	(0.1%)	(18.3%)	(0.7%)	(63.2%)	(5.5%)
SON	–0.427	–0.480	–0.905	–0.897	–0.210	0.477	0.380	–0.480
	(5.2%)	(4.0%)	(0.1%)	(0.1%)	(47%)	(0.9%)	(17.2%)	(5.2%)
DJF	–0.606	–0.731	–0.810	–0.814	–0.302	0.574	0.343	–0.488
	(4.1%)	(1.1%)	(0.1%)	(0.1%)	(40.7%)	(0.3%)	(31.9%)	(1.6%)

[a]For cases 2 and 3 volcanic years are excluded from the El Niño and La Niña composites. Shown in parentheses are the levels of statistical significance of the coefficients derived from Monte Carlo tests.

Niño and La Niña composites provide us the basis to utilize certain statistical tools to extract the signals of El Niño and/or La Niña events from the observed surface temperature anomalies after volcanic eruptions. The singular value decomposition method [*Bretherton et al.,* 1992] is one such statistical tool.

5. SVD Analyses of Surface Temperature Anomalies

5.1. The Tool

SVD analysis [*Bretherton et al.,* 1992] decomposes the cross-covariance matrix of two data fields and identifies the pairs of spatial patterns that explain, as much as possible, the mean-squared temporal covariance between the two fields. It can explain the maximum possible fraction of the cumulative squared covariance with fewer leading modes than any other tool used to isolate coupled modes of variability between the time series of two fields. The method has been applied, for instance, by *Wallace et al.* [1992] to study the coupled variability between wintertime North Pacific SST and 500-hPa heights and by *Ting and Wang* [1997] to study the relation between the summertime precipitation over the United States Great Plains and the North Pacific SST.

5.2. Application

Since our purpose in performing the SVD analysis is to detect the signals of El Niño and La Niña events in the observed surface temperature anomalies, we confine the spatial domain of the first (right-hand) field, the SST anomalies, to be in the tropical Pacific (30°S–30°N, 120°E–80°W) (Figure 3). There are 478 oceanic points in this

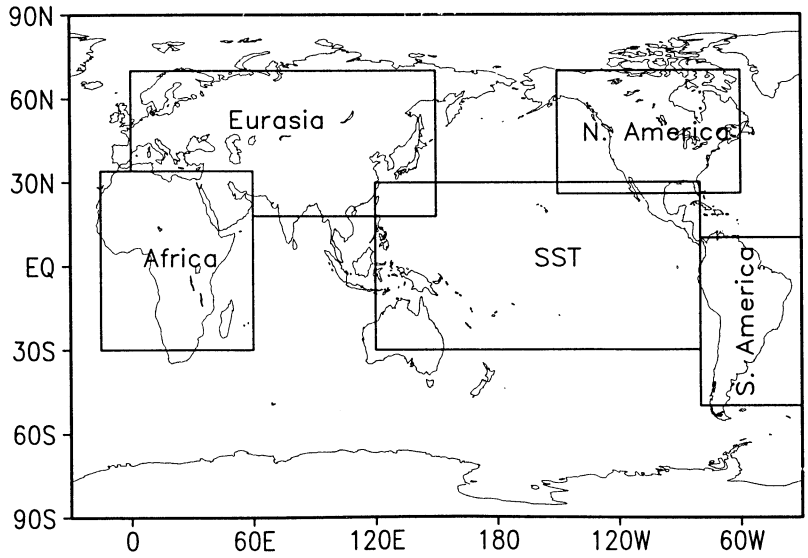

Figure 3. Areas of SST anomalies over the tropical Pacific and SAT anomalies over Eurasia, North America, South America, and Africa used for the SVD analyses.

domain in our 4° x 5° resolution. We chose the SAT anomalies over land to be the left-hand field, and further divided the field into four geographical regions: Eurasia (0°–60°E, 34°–70°N and 60°–150°E, 18°–70°N; 346 points), North America (60°–150°W, 26°–70°N; 168 points), South America (30°–80°W, 50°S–10°N; 111 points), and Africa (15°W–60°E, 30°S–34°N; 195 points) (Figure 3). An SVD analysis was performed for each region and for each season by using the SST anomalies in the tropical Pacific and the SAT anomalies over land.

5.3. Results

We present in Table 3 the fraction of the squared covariance explained by each of the first three pairs of patterns (modes) relative to the cumulative squared covariance of all patterns (FSC_k), together with the percent of the squared variance of the SAT and SST fields explained by each mode k, for the SVD analysis performed for the pair of fields between the Pacific SST and the SAT over each of the four continental regions, and for the DJF and JJA seasons (results for the MAM and SON seasons are not shown). For all the cases listed in Table 3, mode 1 explains a larger percent of the squared variance of the SST field than do modes 2 and 3. Analysis of the homogeneous correlation maps of the SST anomalies (not shown), which are the correlation coefficients (ρ: $-1 \le \rho \le 1$) between the time series of SST field and the time-dependent expansion coefficients of the SST field, shows that only mode 1 of the SST anomalies has a statistically significant SST variance over the central and eastern tropical Pacific, which corresponds to the dominant SST variations associated with ENSO events. *Ting and Wang* [1997] correlated the Pacific SST anomalies with North American precipitation in JJA by using SVD analysis and found that only the first mode of the SST anomalies in the tropical Pacific represents the ENSO-related SST variations. Since our goal is to identify the influence of SST variations associated with ENSO events on SAT over land, we focus in the following on the first mode of the SVD analysis. We concentrate on the Eurasian and North American regions and the DJF and JJA seasons.

Figure 4 shows the leading mode heterogeneous correlation maps (ρ: $-1 \le \rho \le 1$) for SAT and the scaled leading mode patterns for SST from the SVD analyses between SAT anomalies over North America and SST anomalies in the tropical Pacific in JJA and DJF seasons. Figure 5 is the same as Figure 4, except for the SVD analyses between SAT anomalies over Eurasia and SST anomalies in the tropical Pacific. Here heterogeneous means the correlation between the time series of SAT anomalies at each grid point and the time-dependent expansion coefficient (principal component) of the SST field. The heterogeneous correlation map indicates how well the SAT field can be predicted by the leading mode SST field. The Student t test has been used to examine the statistical significance of the correlation coefficients for each grid point. The scaled pattern shows the typical magnitude and distribution of SST anomalies associated with the leading mode of SST. The percent variance explained by the leading mode relative to its total variance for each field is shown on the top of each panel.

In JJA, the leading mode FSC_1 equals 30.1%. The SAT over central and eastern North America is negatively correlated to the SST in the tropical Pacific, and the correlation coefficients are statistically significant at better than the 10% level over most of the region (shown by shading in Figure 4). SAT over western and southern North America is positively correlated to the SST but is not statistically significant. This leading mode of SAT anomalies explains 30.2% of SAT's own squared variance. As expected, the pattern of the leading mode SAT anomaly broadly resembles the distributions of SAT anomalies for the El Niño and La Niña composites in JJA over North America (Figures 2a and

Table 3. Percent Squared Covariance Explained by Each of the First Three Pairs of Patterns (FSC_k) and the Percent of the Squared Variance of the SAT and SST Fields Explained by Each Mode k

Covariance/Variance Explained, %	JJA			DJF		
	Mode 1	Mode 2	Mode 3	Mode 1	Mode 2	Mode 3
			North America			
FSC_k	30.1	14.6	9.8	29.5	21.0	8.9
SAT	30.2	11.0	14.9	32.0	18.4	14.8
SST	20.1	13.1	5.7	18.6	17.6	5.2
			Eurasia			
FSC_k	19.0	13.6	9.4	26.9	15.2	10.0
SAT	11.6	15.9	9.0	14.2	21.7	16.9
SST	28.2	9.7	7.3	32.5	9.4	4.4
			Africa			
FSC_k	27.7	11.9	7.6	39.2	16.1	7.0
SAT	29.7	8.3	8.7	29.9	22.9	8.2
SST	25.9	14.0	5.1	32.2	14.2	5.5
			South America			
FSC_k	46.3	12.3	9.0	50.8	12.0	9.8
SAT	37.9	20.1	7.0	39.2	22.8	6.7
SST	31.2	5.8	10.4	34.6	6.5	12.4

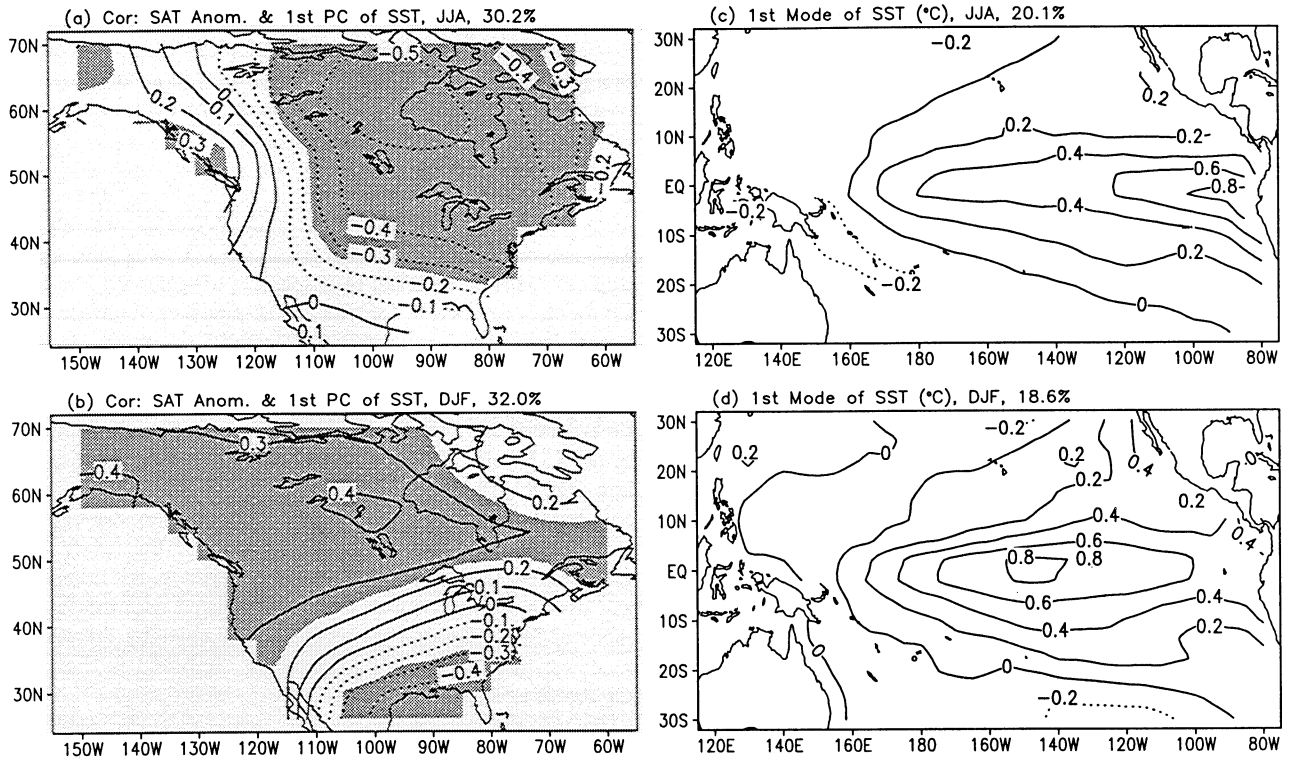

Figure 4. (a, b) Leading mode heterogeneous correlation maps for SAT and (c, d) the scaled leading mode patterns for SST from the SVD analysis between the SAT anomalies over North America and the SST anomalies in the tropical Pacific for (a, c) JJA and (b, d) DJF. In Figures 4a and 4b, correlation coefficients that are statistically significant at better than the 10% level are shaded. The percent variance explained by the leading mode relative to its total variance for each field is shown on the top of each panel.

2b). The leading mode of SST anomaly represents the observed dominant SST variability in the tropical Pacific associated with El Niño and La Niña events and explains 20.1% of the squared variance of the SST field.

In DJF, the leading mode FSC_1 equals 29.5%. SAT over all but southeastern North America is positively correlated with the SST in the tropical Pacific. This leading mode of SAT anomalies explains 32.0% of SAT's own squared variance. The pattern of the leading mode SAT anomalies also resembles the distributions of SAT anomalies for the El Niño and La Niña composites in DJF over North America (Figures 2d and 2e).

For Eurasia (Figure 5), in both JJA and DJF, the correlation is significant only over northeastern and southeastern Eurasia. The influence of the SST in the tropical Pacific on the SAT over Europe is weak. The pattern of the leading mode SAT anomalies in DJF resembles the distributions of SAT anomalies for the El Niño and La Niña composites over Eurasia (Figures 2d and 2e). In JJA the resemblance is less prominent.

So far we have found the patterns of the leading mode SAT anomalies that can be explained by the dominant variability of the SST in the tropical Pacific. Now, we project these leading modes onto specific years to obtain the contributions of the SST in the tropical Pacific to the observed SAT anomalies in those years by multiplying the leading mode SAT anomalies by the expansion coefficients of the SST field.

Figure 6 presents the seasonal mean SAT anomalies over North America for the high-pass-filtered SAT anomalies, the projection of the leading mode SAT anomalies from the SVD analyses, and the differences (residuals) between the high-pass-filtered SAT anomalies and the projected SAT anomalies, for each of the four seasons, DJF 1991-1992, JJA 1992, DJF 1992-1993 and JJA 1993. On each panel, areas with values exceeding 1.3σ in magnitude are shaded, where σ is the standard deviation of the high-pass-filtered seasonal mean SAT anomalies at each grid point between 1950 and 1997. For a time series with a normal distribution and with no autocorrelation, about 10% of the data fall outside of the range $\{-1.3\sigma, 1.3\sigma\}$. Therefore the shaded areas are statistically significant at better than the 10% level. The observed SAT in DJF 1991-1992 was above normal over North America except over the northeastern portion. About +4.0°C anomalies were found over the central United States. In DJF 1992-1993 the observed SAT was below normal, with a minimum of –2.5°C found over the United States and eastern Canada, and above normal over central and western Canada and Alaska, with a maximum of about 2.5°C. In JJA 1992 the observed SAT was below normal over the entire North American continent, with the largest cooling of about –2.5°C over the central United States. In JJA 1993 the observed SAT was below normal, with a minimum of about –2.5°C found over western North America, and above normal over eastern North America, with a maximum of about 1.5°C.

By *Trenberth*'s [1997] definition, two El Niño events occurred around the Pinatubo eruption. The first one occurred between March 1991 and July 1992, with the Niño 3.4 index reaching a maximum of about 1.5°C in DJF 1991-1992. The

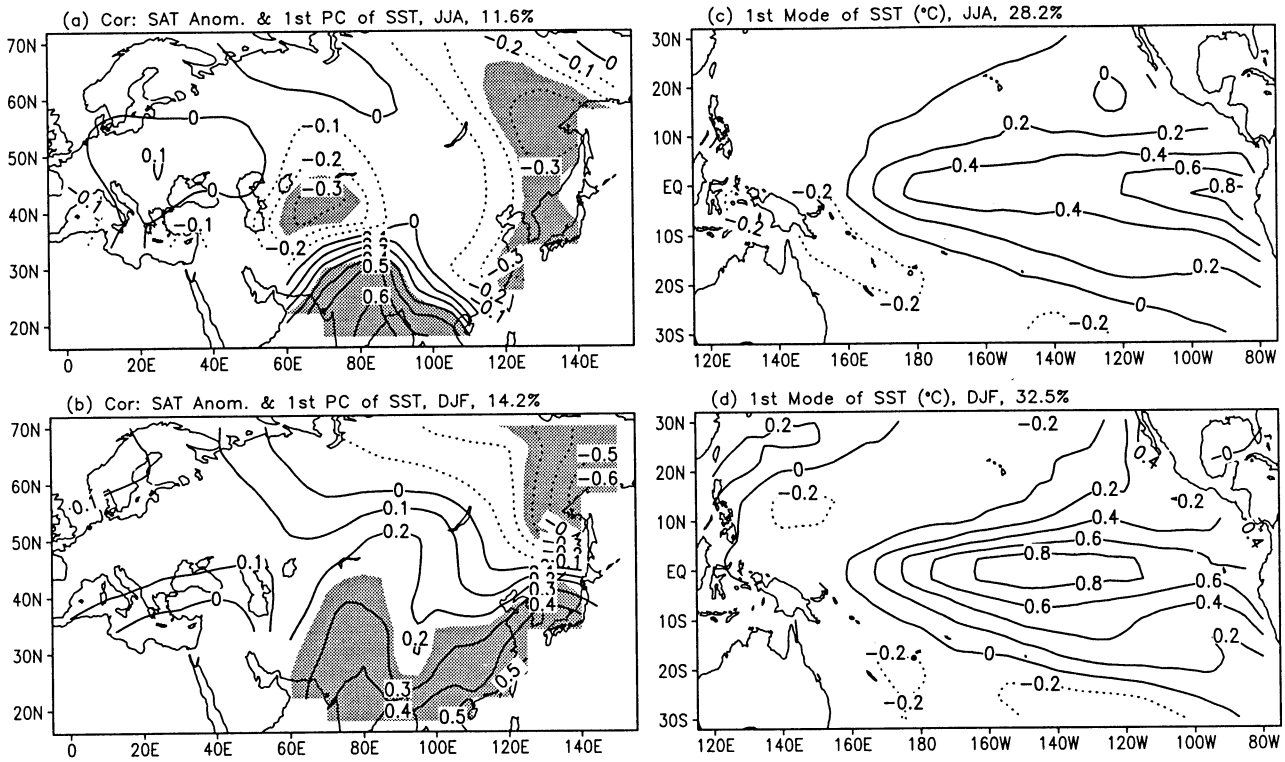

Figure 5. Same as Figure 4, except for the SAT anomalies over Eurasia.

second one occurred between February 1993 and September 1993, with a much weaker maximum peaking in MAM 1993. The projections of the leading mode SAT anomalies in Figure 4 indicate that the 1991-1992 El Niño event contributed significantly to the observed SAT anomalies over North America, while the 1993 El Niño event made no significant contributions. The 1991-1992 El Niño event led to a 0.5°C increase of the SAT over the U.S. Great Plains and Canada in DJF 1991-1992, and led to a –0.5°C to –1.5°C decrease of the SAT over most of North America in JJA 1992. Consequently, the observed negative anomalies over central and eastern Canada in the original high-pass-filtered field become positive anomalies in the residual field in JJA 1992. Over the entire North American continent, minor cooling occurred in DJF 1992-1993 and minor warming occurred in JJA 1993 on the projected fields of the leading mode SAT anomalies.

For Eurasia (Figure 7), large warming was found in both DJF 1991-1992 and DJF 1992-1993, and large cooling was found in JJA 1992 and JJA 1993 in the high-pass-filtered fields. However, the signal-to-noise ratios for the winter warming are low over most regions. The contributions of the 1991-1992 El Niño and 1993 El Niño to the observed temperature anomalies are negligible in the Northern Hemisphere winters but are relatively large in the Northern Hemisphere summers, reaching –0.16°C in JJA 1992 and –0.17°C in JJA 1993 averaged over the domain.

To present the SVD analyses performed for the MAM and SON seasons and for the South American and African continents, in addition to the above North American and Eurasian continents, we calculated the area mean SAT anomalies over each of the four continents for all the seasons between JJA 1991 and JJA 1994. Figure 8 depicts for each continent the time evolutions of the area means of the high-pass-filtered SAT anomalies and the residual SAT anomalies. The residual represents the SAT anomaly with the ENSO signals removed. Figure 8 also shows the averages of SAT anomalies over the four continents and the index of global mean land-ocean surface temperature anomalies, ΔT_s, which is composed of the seasonal mean high-pass-filtered SAT anomalies over the four continents and the seasonal mean high-pass-filtered SST anomalies over the ocean, except the Arctic and the Southern Ocean near Antarctica.

Over Eurasia and North America the SAT had a maximum change of about ±1°C during the 2 years following the June 1991 Pinatubo eruption. The signals of ENSO events were negligible over Eurasia but were important over North America. Over North America, the observed maximum coolings occurred in JJA 1992 and DJF 1993-1994 for the original high-pass-filtered data but in SON 1992 and SON 1993 for the residuals, in which the ENSO signals have been removed. Over Eurasia, SAT increased by 0.5°C in DJF 1991-1992 and 1°C in DJF 1992-1993 and decreased in other seasons, with a maximum cooling of about –1°C in SON 1992 and SON 1993. The influences of the 1991-1992 and 1993 El Niño events were insignificant over Eurasia. Over North America, ENSO signals were rather strong. Temperature anomalies induced by the ENSO events were about ±0.5°C.

Over South America and Africa, the SAT had maximum changes of about ±0.5°C before early 1993. The influences of the El Niño events were noticeable over both continents. Over South America, a maximum warming of about 0.4°C occurred in MAM 1992, which was caused by the 1991-1992 El Niño event, and a maximum cooling of about –0.4°C occurred in SON 1992, to which the El Niño event contributed about 25%. Over Africa, a maximum cooling of about –0.6°C to –0.7°C occurred in DJF 1991-1992 and DJF 1992-1993. In DJF

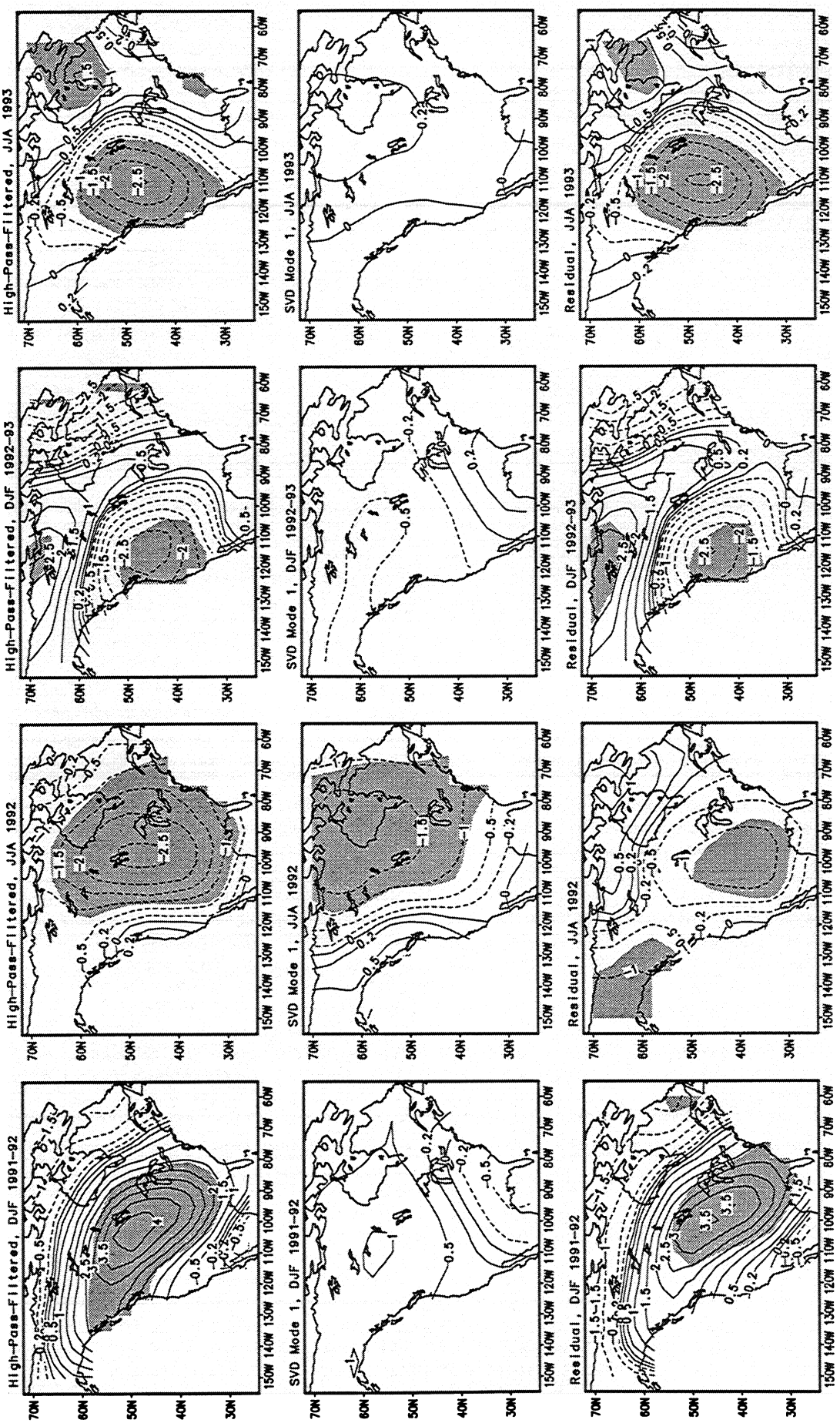

Figure 6. SAT anomalies (degrees Celsius) over North America in DJF 1991-1992, JJA 1992, DJF 1992-1993, and JJA 1993 for (top) the high-pass-filtered data, (middle) the projections of the leading mode SAT anomalies, and (bottom) the differences (residuals) between the high-pass-filtered SAT anomalies and the projections. The contour interval is 0.5°C with the ±0.2°C lines added. Negative values are dashed. Areas with anomalies exceeding 1.3σ in magnitude are shaded, where σ is the standard deviation of the high-pass-filtered seasonal mean SAT anomalies at each grid point between 1950 and 1997.

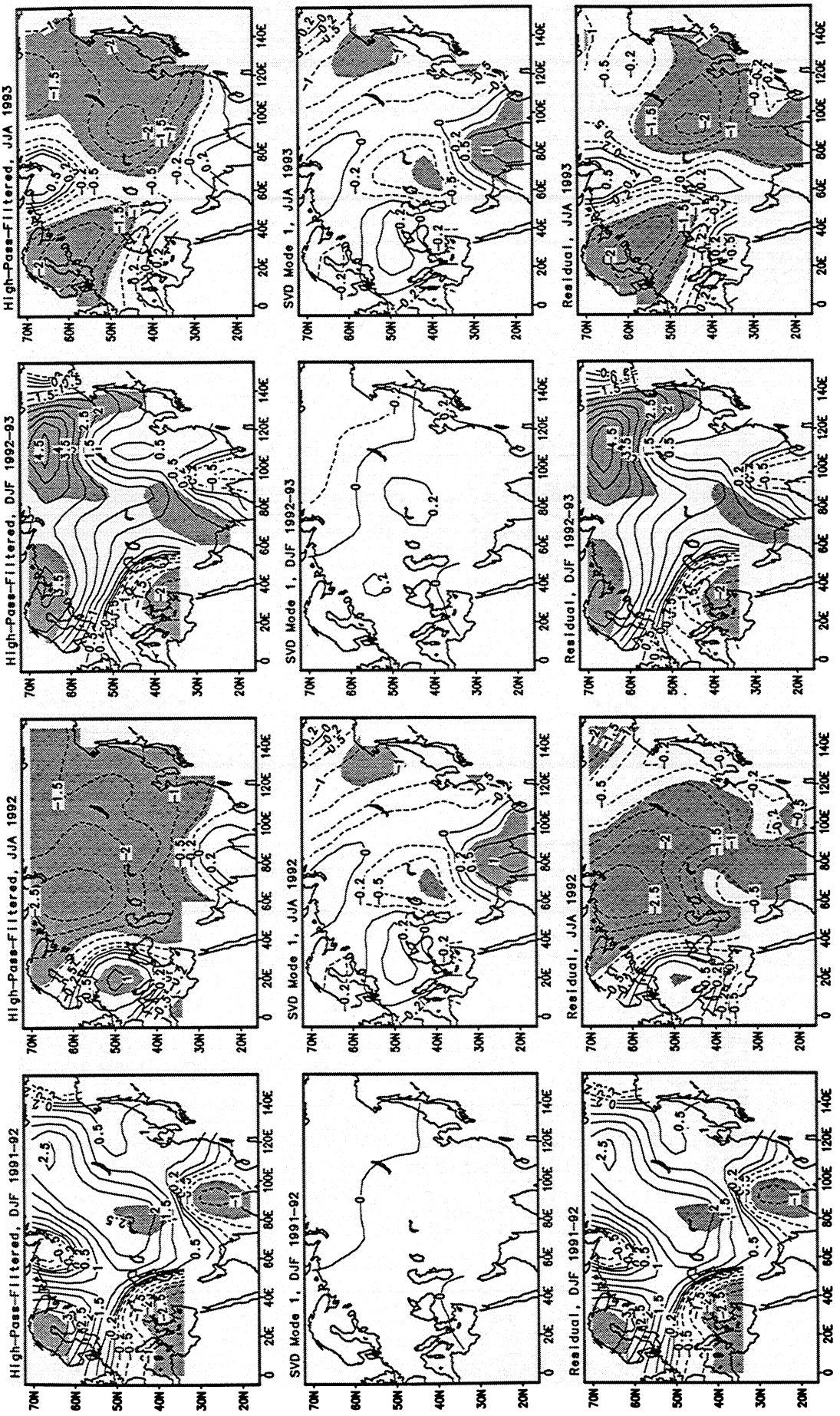

Figure 7. Same as Figure 6, except for Eurasia.

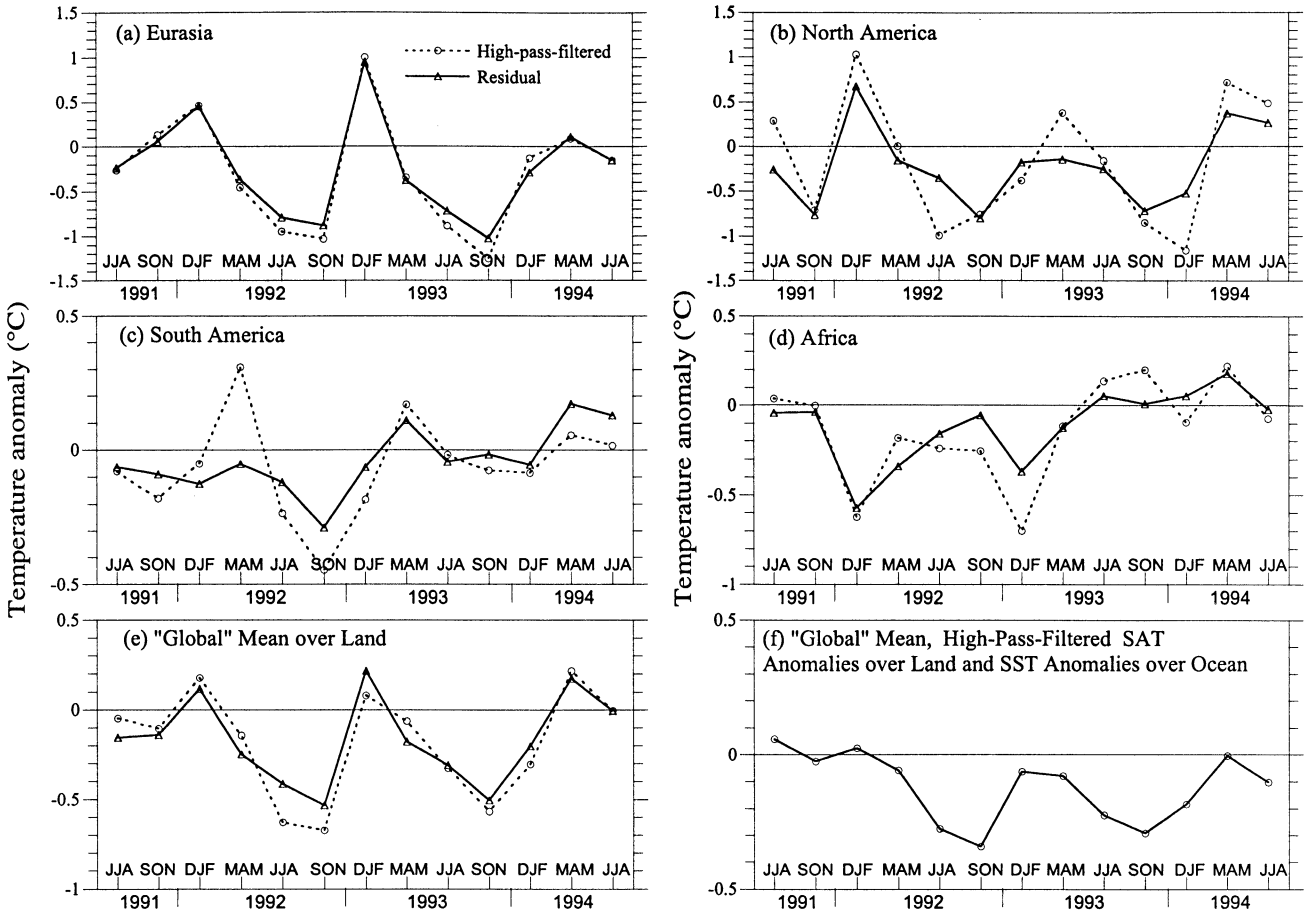

Figure 8. Time evolutions of mean SAT anomalies (degrees Celsius) averaged over (a) Eurasia, (b) North America, (c) South America, and (d) Africa for the high-pass-filtered SAT anomalies and the residual SAT anomalies after the ENSO signals have been removed. (e) Averages over the four continents. (f) Index of global mean land-ocean surface temperature anomalies, ΔT_s, which includes the high-pass-filtered SAT anomalies over the four continents and the high-pass-filtered SST anomalies over the ocean.

1992-1993, 50% of the observed cooling was attributed to the influence of the ENSO events.

The above analyses indicate that the changes of SAT over land induced by the SST anomalies in the tropical Pacific and by the Pinatubo eruption are inhomogeneous in space and asynchronous in time. With the signals of the ENSO events removed, the mean SAT over the four continents (Figure 8e) increased by 0.1°-0.2°C in DJF 1991-1992 and DJF 1992-1993, and decreased by 0.5°-0.6°C in SON 1992 and SON 1993. The global mean land-ocean temperature index, ΔT_s (Figure 8f) also shows maximum cooling in SON 1992 (–0.34°C) and SON 1993 (–0.29°C).

To check how well the SVD leading modes represent the observed SAT variability, which can be explained by ENSO events, we plot in Figure 9 the time evolution of the leading mode SAT anomalies from MAM 1950 through DJF 1996-

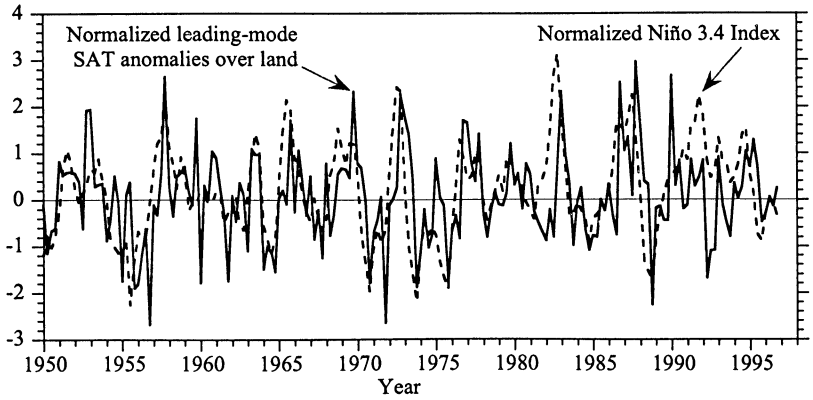

Figure 9. Time evolutions of the projected leading mode SAT anomalies (solid line) from the SVD analysis, averaged over Eurasia, North America, South America, and Africa, and the Niño 3.4 index (dashed line). Each time series is normalized by its standard deviation.

1997 averaged over Eurasia, North America, South America, and Africa, together with the Niño 3.4 index. Each time series is normalized by its own standard deviation. We can see that the peaks and troughs of the SAT anomalies generally follow the Niño 3.4 index. However, in certain years there are phase shifts, and the magnitudes of the SAT anomalies are not in proportion to the magnitudes of the Niño 3.4 index. The correlation coefficient between these two time series is 0.46. Nevertheless, this correlation coefficient is still much higher than that between the Niño 3.4 index and the high-pass-filtered SAT anomalies over the four continents before the decomposition, which is only 0.21.

6. Conclusion

We have analyzed the observed SAT anomalies over land and SST anomalies for 1950-1997. Composite analyses show that over the ocean the distribution of SST anomalies for the El Niño composite is opposite to that for the La Niña composite, not only in the middle to eastern tropical Pacific, but also in some other regions of the ocean. The pattern of SST anomalies for each composite does not change much from season to season. Over land the distribution of SAT anomalies for the El Niño composite is opposite to that for the La Niña composite in most regions, and the patterns of SAT anomalies change from season to season. This feature is more distinct over North America than over the other continents. Over North America, negative SAT anomalies dominate for the El Niño composite in JJA and for the La Niña composite in DJF, and positive SAT anomalies dominate for the La Niña composite in JJA and for the El Niño composite in DJF.

The volcano composite is different from either the El Niño composite or the La Niña composite. We used SVD analysis to detect and remove the signals of the 1991-1992 and 1993 El Niño events from the observed SAT anomalies over Eurasia, North America, South America, and Africa for the 3 years following the Pinatubo eruption. It is found that ENSO signals were weak over Eurasia but relatively strong over the other continents. Over North America, the 1991-1992 El Niño event contributed more than 50% to the observed total cooling of about –1.0°C in JJA 1992. Averaged over the four continents, maximum coolings of about –0.5°C occurred in SON 1992 and SON 1993 with the ENSO signals removed.

Removing the ENSO signals enables us to better understand the patterns and time evolution of the temperature changes induced by the Pinatubo eruption. However, some limitations of this approach need to be pointed out. First, in principle, the SVD analysis is a linear operator. For each mode the response of the left-hand field to the right-hand field is proportional to the magnitude of the right-hand field. Though the amplitude of the atmospheric response to the amplitude of the SST anomalies in the tropical Pacific grows linearly to first order, an important departure from this linear response exists [*Kumar and Hoerling*, 1998]. The atmospheric responses to warm-event SST anomalies in the tropical Pacific are stronger than the atmospheric responses to cold-event SST anomalies [*Hoerling et al.*, 1997; *Kumar and Hoerling*, 1998]. The SVD analysis cannot capture this nonlinearity. Second, the observed data used here extend from 1950 to 1997. There are only 48 points in the time domain in contrast to hundreds of data points in the space domain. Spuriously high correlation coefficients with rather low statistical significance might be produced between any two fields with mismatched degrees of freedom in space and time. Third, with the ENSO signals being removed, the residual temperature anomalies still cannot be attributed solely to the influence of the Pinatubo eruption. Other factors such as the phase change of the quasi-biennial oscillation, ozone depletion, and SST variations other than ENSO events also contributed to the observed temperature anomalies. Our effort is limited to isolating the signals that can be explained by the variability of the SST in the eastern tropical Pacific.

Acknowledgments. This study was supported by the National Science Foundation under grant ATM-9522681. We thank Sergey Malyshev for assistance in preparing the figures and typesetting the paper.

References

Andronova, N. G., and M. E. Schlesinger, Causes of global temperature changes during the 19th and 20th centuries, *Geophys. Res. Lett., 27*, 2137-2140, 2000.

Andronova, N. G., E. Rozanov, F. Yang, M. E. Schlesinger, and G. L. Stenchikov, Radiative forcing by volcanic aerosols from 1850 through 1994, *J. Geophys. Res., 104*, 16,807-16,826, 1999.

Angell, J. K., Impact of El Niño on the delineation of tropospheric cooling due to volcanic eruptions, *J. Geophys. Res., 93*, 3697-3704, 1988.

Bluth, G. J. S., S. D. Doiron, C. C. Schnetzler, A. J. Krueger, and L. S. Walter, Global tracking of the SO_2 clouds from the June, 1991 Mount Pinatubo eruption, *Geophys. Res. Lett., 19*, 151-154, 1992.

Bretherton, C. S., C. Smith, and J. M. Wallace, An intercomparison of methods for finding coupled patterns in climate data, *J. Clim., 5*, 541-560, 1992.

Duchon, C. E., Lanczos filtering in one and two dimensions, *J. Appl. Meteorol., 18*, 1016-1022, 1979.

Graf, H. F., I. Kirchner, A. Robock, and I. Schult, Pinatubo eruption winter climate effects: Model versus observations, *Clim. Dyn., 9*, 81-93, 1993.

Groisman, P. Y., Possible regional climate consequences of the Pinatubo eruption: An empirical approach, *Geophys. Res. Lett., 19*, 1603-1606, 1992.

Hansen, J., A. Lacis, R. Ruedy, and M. Sato, Potential climate impact of Mount Pinatubo eruption, *Geophys. Res. Lett., 19*, 215-218, 1992.

Hansen, J., R. Ruedy, J. Glascoe, and M. Sato, GISS analysis of surface temperature change, *J. Geophys. Res., 104*, 30,997-31,022, 1999.

Hoerling, M. P., A. Kumar, and M. Zhong, El Niño, La Niña, and the nonlinearity of their teleconnections, *J. Clim., 10*, 1769-1786, 1997.

Kirchner, I., and H. F. Graf, Volcanoes and El Niño: Signal separation in Northern Hemisphere winter, *Clim. Dyn., 11*, 341-358, 1995.

Kirchner, I., G. L. Stenchikov, H. F. Graf, A. Robock, and J. C. Antuna, Climate model simulation of winter warming and summer cooling following the 1991 Mount Pinatubo volcanic eruption, *J. Geophys. Res., 104*, 19,039-19,055, 1999.

Kumar, A., and M. P. Hoerling, Annual cycle of Pacific-North America seasonal predictability associated with different phases of ENSO, *J. Clim., 11*, 3295-3308, 1998.

Mass, C. F., and D. A. Portman, Major volcanic eruptions and climate: A critical evaluation, *J. Clim., 2*, 566-593, 1989.

McCormick, M. P., L. W. Thomason, and C. R. Trepte, Atmospheric effects of the Mt. Pinatubo eruption, *Nature, 373*, 399-404, 1995.

Parker, D. E., H. Wilson, P. D. Jones, J. R. Christy, and C. K. Folland, The impact of Mount Pinatubo on world-wide temperatures, *Int. J. Climatol., 16*, 487-497, 1996.

Reynolds, R. W., and T. M. Smith, Improved global sea surface temperature analyses using optimum interpolation, *J. Clim., 7*, 929-948, 1994.

Reynolds, R. W., and T. M. Smith, A high-resolution global sea surface temperature climatology, *J. Clim., 8*, 1571-1583, 1995.

Robock, A., and J. Mao, The volcanic signal in surface temperature observations, *J. Clim., 8*, 1086-1103, 1995.

Smith, T. M., R. W. Reynolds, R. E. Livezey, and D. C. Stokes,

Reconstruction of historical sea surface temperature using empirical orthogonal functions, *J. Clim.*, *9*, 1403-1420, 1996.

Stenchikov, G. L., I. Kirchner, A. Robock, H.-F. Graf, J. C. Antuña, R. G. Grainger, A. Lambert, and L. Thomason, Radiative forcing from the 1991 Mt. Pinatubo volcanic eruption, *J. Geophys. Res.*, *103*, 13,837-13,857, 1998.

Ting, M., and H. Wang, Summertime United States precipitation variability and its relation to Pacific sea surface temperature, *J. Clim.*, *10*, 1853-1873, 1997.

Trenberth, K. E., The definition of El Niño, *Bull. Am. Meteorol. Soc.*, *78*, 2771-2777, 1997.

Wallace, J. M., C. Smith, and C. S. Bretherton, Singular value decomposition of wintertime sea surface temperature at 500-mb height anomalies, *J. Clim.*, *5*, 561-576, 1992.

Yang, F., Radiative forcing and climatic impact of the Mount Pinatubo volcanic eruption, Ph.D. dissertation, 219 pp., Univ. of Ill. at Urbana-Champaign, Urbana, 2000.

Yang, F., M. E. Schlesinger, and E. Rozanov, Description and performance of the UIUC 24-layer stratosphere/troposphere general circulation model, *J. Geophys. Res.*, *105*, 17,925-17,954, 2000.

M. E. Schlesinger, Climate Research Group, Department of Atmospheric Sciences, University of Illinois at Urbana-Champaign, Urbana, IL 61801. (schlesin@atmos.uiuc.edu)

F. Yang, EMC/NCEP, 5200 Auth Road, Camp Springs, MD 20746. (fyang@ncep.noaa.gov)

(Received October 12, 2000; revised February 8, 2001;
accepted February 15, 2001.)